# Mechanisms of control authority by Nanosecond Pulsed Dielectric Barrier Discharge Actuators on Flow Separation

*Christoforos Skourides, Dimitrios Nyfantis, Pénélope Leyland⋆ and Philip Peschke⋆⋆*
*⋆ GR-SCI-IAG, IGM; ⋆⋆ GR-SCI-GTT, IGM*
*Station 9, Ecole Polytechnique Fédérale de Lausanne (EPFL), CH-1015 Lausanne, Switzerland*
†Christoforos Skourides, christoforos.skourides@epfl.ch

## Abstract

The mechanisms that should be considered for separation flow control applications of nanosecond pulsed DBD actuators was investigated on a NACA 0015 profile for velocities of $10\,m/s$ ($Re = 100,000$) and $20\,m/s$ ($Re = 200,000$). The dominant frequencies existing in the flow were measured. Moderate voltage levels were applied (4 and $7\,kV$) and the actuator was operated at the frequencies which were most dominant in the flow and compared with known effective frequencies from literature. In all cases influences by the actuator on the structures of the flow were observed and the operation of the actuator at the dominant flow frequencies of a stalled airfoil was shown to give control authority .

## Nomenclature

| | | |
|---|---|---|
| $U_\infty$ | Freestream velocity | $[\,m/s\,]$ |
| $\alpha$ | angle of attack | $[^\circ]$ |
| $c$ | Model chord length | $[\,mm\,]$ |
| $C_p$ | Coefficient of pressure | [-] |
| $f$ | Frequency of actuation | $[\,Hz\,]$ |
| $F_c^+$ | Reduced frequency based on model chord | [-] |
| $Re$ | Reynolds number based on model chord and $U_\infty$ | [-] |
| $s$ | Model span | $[\,mm\,]$ |
| $U$ | Magnitude of the applied voltage | $[\,kV\,]$ |

## 1. Introduction

The ability to manipulate a flow field to improve the efficiency and performance of airfoils is of great technological importance. Efficient flow control devices can be used to modify the laminar-turbulent transition inside the boundary layer, to prevent separation, to reduce drag and enhance airfoil lift. They may also be used to stabilise and mix airflow in order to reduce unsteadiness which generates unwanted vibrations, noise and energy losses.[1–3]

Both active and passive flow control devices can be used to control the flow over an airfoil. Passive techniques for flow control modify a flow without any external energy expenditure, such as geometric shaping to manipulate the pressure gradient, the use of fixed mechanical vortex generators for separation control or segmented leading edge slats. Though these devices are efficient in augmenting the lift, they create significant increases in mechanical complexity, manufacturing cost, weight and can induce a parasitic drag.[4,5]

There are several mechanisms by which active flow control techniques act; they include specifically aligned vortex generation or wall jets, the introduction of additional momentum or energy into the flow. A localised periodic excitation close to potential separation locations can be used to impart global changes to separated flow fields, typically by flow perturbation. These perturbations can be achieved by various methods, most often by means of piezoelectric, electromagnetic and electrostatic devices, which are operated by an electromechanical driver. Compared to passive control techniques, these devices offer a significant reduction in weight, mechanical complexity and parasitic drag; however they possess limited bandwidth and are subject to mechanical failure as the driver is operated at resonance in order to meet the amplitude requirements necessary at those flight speeds.[6,7,9]

In the course of the past decade, the use of plasma actuators for active flow control has been implemented by many researchers and has become one of the most booming realms of aerodynamics.[8,10,11] Dielectric barrier discharge

(DBD) actuators are composed of at least two electrodes separated by a dielectric material between which a high voltage is applied, creating a plasma sheet.[11–13] Various electrode geometries are possible, and different signals can be used to excite the actuator. Flow control with plasma is appealing as the actuators used are entirely surface mounted, lack any mechanical parts and possess high bandwidth while requiring relatively low power to be actuated.[8,14] The response time is very short, enabling real-time flow control. The effectiveness of DBD actuators has been proven for velocities up to $Ma = 0.75$, with different geometries or actuation signals showing superiority in different flow regimes.[15–18] Two types of plasma generation are typically used for DBD actuators: A/C power supplies, providing a sinusoidal signal to the electrode setups, for which the dominant effects are the presence of a low-speed ionic wind by the plasma in the near -wall region, with injection of momentum in the boundary layer like a wall-jet, and the other hand, nano-second pulsed power signals, that generate a localised injection of energy, a small vortex generation and a pulsing micro-shock wave,.[8,11]

Typically the actuation frequencies are expressed in terms of reduced frequency $F_c^+$ based on chord and freestream velocity. A preference for low frequency actuation is generally seen, with maximum flow attachment obtained in the range of $F_c^+ = 1$ to 2 for a NACA 0015 airfoil.[9,20] As the value of $F_c^+$ is increased the influence of the plasma on the flow attachment weakens. Two mechanisms of separation flow control have been reported as being effective in NS-DBD actuators. The first mechanism operates at high frequency, and is connected to the instability of the boundary layer and its turbulisation. The second mechanism corresponds to the instability of the separation shear layer and the effect on its shedding structures and operates at lower frequencies. The excitation of these structures induces efficient entrainment of the flow and induces the most effective flow attachment. If the discharge power is not sufficiently large to effectively excite the shear layer, only the first mechanism remains.[15,19–23] These shedding structures have been observed also in PIV measurements for relatively low-speed flow (up to 60 m/s) in a study by Little et. al.[20] However, other frequencies of actuation are thought to give significant control authority.Since the mechanism of control is the excitation of some inherent flow instabilities present in the flow field, in order to manipulate the vortex structures of interest the frequency of actuation needs to correspond to the frequencies of these instabilities.[25]

This paper details the investigation of the mechanisms that allow for control authority for an asymmetric nanosecond pulsed dielectric barrier discharge (NS-DBD) actuator on the aerodynamic characteristics of a NACA 0015 airfoil profile. Experiments were performed in a low-speed wind tunnel at freestream flow speeds of 10 and 20 $m/s$ at angles of attack of 16° and 24°. Pressure taps along the profile chord located at mid-span on both the suction and pressure sides of the airfoil were used also to determine the effectiveness of the actuator at various frequencies. Hot wire anemometry was performed with the aim of identifying dominant frequencies in the flow field over the stalled profile. Furthermore, PIV measurements were taken to identify how different actuation frequencies affect the existing structures in the flow field.

## 2. Experimental Setup

### 2.1 Model

The model used throughout the experiments is a NACA 0015 profile, with a chord length of 150 $mm$ and a span of 450 $mm$. It incorporates a recess 0.8 $mm$ deep around the leading edge, stretching from $x/c = 0.09$ on the suction side to $x/c = 0.11$ on the pressure side. Its length along the span of the model is 360 $mm$. This recess allowed for flush actuator integration so as to minimize surface discontinuities during the plasma experiments. Twenty one pressure taps were incorporated into the model at locations shown in Figure 1. Only sixteen of these could be used as four of the taps were located within the recessed area that was covered during the experiments on the model by the actuator upper electrode, while another pressure tap just upstream of the trailing edge of the airfoil could not be used due to data acquisition system.

Two Scanivalve DSA3217 pressure sensors were used to measure the static pressure from the seventeen operational pressure taps along the model chord. The pressure was sampled at a frequency of 20 $Hz$ and averaged over a sample of 100 measurements. The static and total pressures of the freestream flow were measured from the pitot-tube by two Druck LPM 5480 pressure sensors sampled at a frequency of 50 $Hz$ taking a sampling size of 150 measurements.

### 2.2 Wind Tunnel

The experiments were conducted in an open-loop wind tunnel consisting of a modified radial blower driven by a frequency converter controlled 5.5 $kW$ asynchronous motor and connected to an asymmetric wide angle diffuser via a vibration absorber. The air is aspirated in from the laboratory into the tunnel through a dust filter, located in front of the radial blower intake, before eventually being returned to the room via a diffuser. Five screens in the wide angle

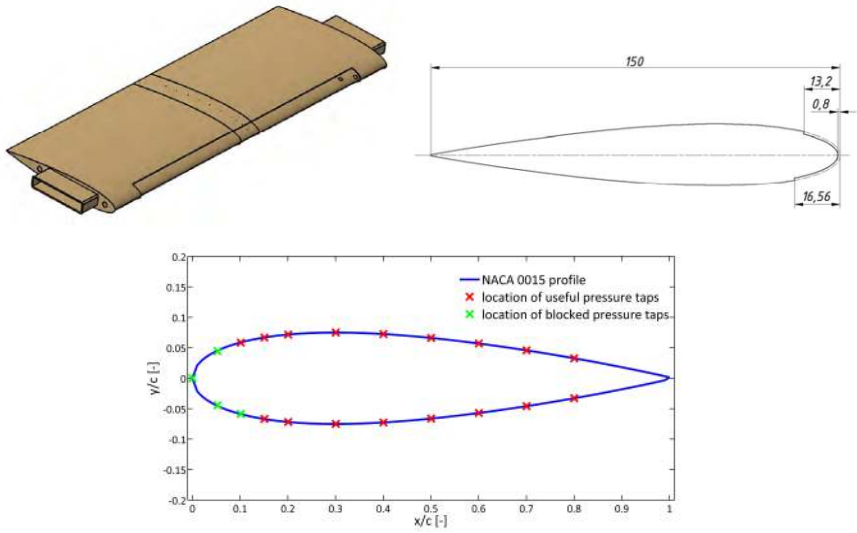


Figure 1: Top: A 3-D view of the model used with a NACA 0015 profile and a cross-section of the model showing the recess in the profile. Below: the profile with the marked pressure tap locations used. The green ones were blocked by the actuator.

diffuser prevent flow separation. In the settling chamber, a honeycomb, dust filter and final screen are installed to smooth out flow inhomogeneities. The modular test section has a cross-section of 450 $mm$ width and 300 $mm$ height. A thermocouple and pitot-static tube are located upstream of the model. The static and total pressures of the freestream flow were measured from the pitot-tube by two Druck LPM 5480 pressure sensors sampled at a frequency of 50 $Hz$ connected to a Tektronix TDS210 two-channel digital oscilloscope in order to compute the freestream velocity. The model was held at the correct angles of attack using two different sets of test-section windows with fixed cut-outs at 16° and 24° .

### 2.3 DBD actuator construction

The DBD actuator was constructed from two copper electrodes separated by a dielectric layer and arranged in an asymmetric manner, as shown in Figure 2. There is a slight overlap between the upper and lower electrodes in order to encourage uniform plasma generation.[10] The encapsulated electrode has a width of 10 $mm$ while the exposed electrode is 4 $mm$ wide. The length of the actuator over the model span, which corresponds to the length of the exposed electrode, is 300 $mm$. The dielectric barrier is composed of four layers of Kapton tape. Each layer has a thickness of 70 $\mu m$ : 25 $\mu m$ Kapton with a 45 $\mu m$ adhesive layer. The plasma forms in the upstream direction over the encapsulated electrode, as seen in Figure 2. Thus the first disturbance encountered by the flow is the plasma itself. The upstream edge of the exposed electrode was located at a distance of 4.5 $mm$ along the chord from the leading edge of the model (at $x/c = 0.03$). As the occurrence of plasma on an airfoil surface induces only a relatively small effect on the airflow, it is clear that to gain any significant advantage from its use considerable leverage should be provided by the flow sensitivity. Many experimental studies[15,19,21,22] have been performed with the aim of determining the optimal location of a NS-DBD actuator on such a profile. These studies have consistently shown that the maximum effect is achieved when the electrodes are positioned such that the discharge zone is located just upstream of the separation point.

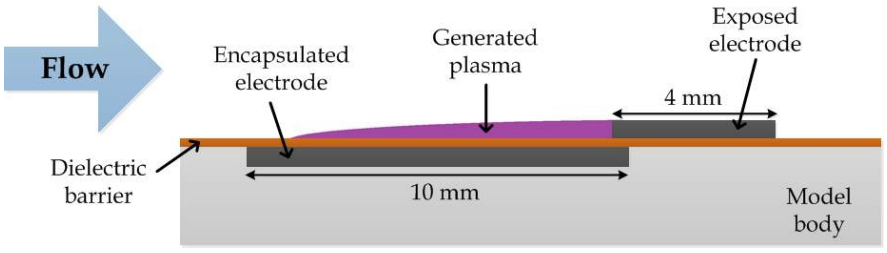


Figure 2: Scheme of the DBD actuator

### 2.4 Power Supply

The core of the power supply used in the experiments is a Behlke HTS111-06-GSM fast high-voltage transistor switch, composed of two identical MOSFET switching paths forming a so-called push-pull circuit. The basic circuit of the power supply is given in Figure 3. A $5V$ DC power supply and a function generator are needed to drive the switch and control the output; the latter serving as a trigger signal. A DC voltage supply provides a constant voltage of up to $10\,kV$, which charges the capacitor C1 with a capacitance of $7000\,pF$. Once the switch opens the DBD actuator sub-circuit, the voltage is primarily provided by the capacitor. Therefore, the DC power supply can operate with a low output current. The current required to charge the capacitor depends on the repetition rate of the output voltage pulse.

The actuator was operated by means of nanosecond pulses generated by a Rhode& Schwarz function generator. The operating regime used was periodic (NS-P), with a constant frequency of pulses fed into the discharge gap at peak voltages of either 4 or $7\,kV$. Although the peak voltage that can be provided by the power supply is $10\,kV$, this value was not attainable during these experiments. Typical waveforms for voltage and current used during the experiments are shown in Figure 4.

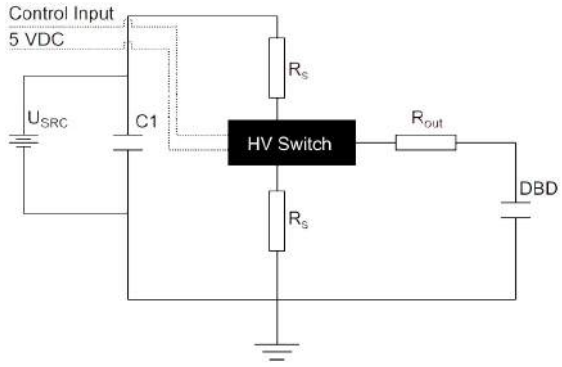


Figure 3: Power Supply setup, from.[17]

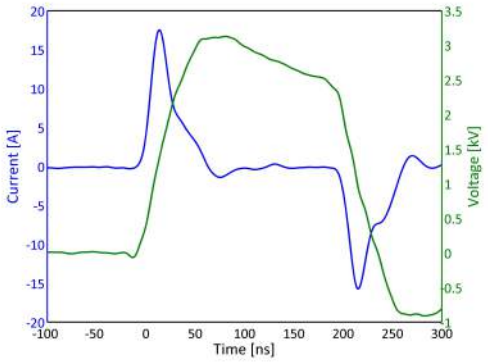


Figure 4: Sample current and voltage waveforms.

### 2.5 Test Conditions

In the baseline experiments, where measurements were performed on the smooth profile, two values of freestream velocity produced by the wind tunnel were investigated: $10\,m/s$ and $20\,m/s$, corresponding to Reynolds numbers relative to the chord of 100,000 and 200,000 respectively. The angles of attack investigated were 16° and 24°.

At a $Re = 100000$ and $\alpha = 16°$ the frequencies tested were $f = 35$, 44.2, 66.6, 133.3, 199.9, 266.6, 500 , 666.6 and $1058\,Hz$ which included the values of reduced frequency of $F_c^+ = 1$, 2 ,3, 4 and 10. At the same $Re$ and $\alpha = 24°$ the frequencies tested were $f = 34$, 66.6, 133.3, 199.9, 266.6, 400 and $700\,Hz$ and included the values of reduced frequency of $F_c^+ = 1$, 2,3 and 4 .

At a $Re = 200000$ and $\alpha = 16°$ the frequencies tested were $f = 33.6$, 41, 133.3, 174.4, 266.6 and 533.3 which which included the values of reduced frequency of $F_c^+ = 1$, 2 ,4. At the same $Re$ and $\alpha = 24°$ the frequencies tested were $f = 69$, 133.3, 266.6, 400, 470, 533.3 and $1333.3\,Hz$ and included the values of reduced frequency of $F_c^+ = 1$, 2,3, 4 and 10 .

The choice for the frequencies was made by examining the power spectra of the velocity field, without plasma actuation, obtained by using Hot Wire Anemometry and including values of reduced frequency that were known to be effective. Further details of this procedure follow in the next section.

## 3. Experimental Techniques

### 3.1 Pressure Measurements

Two Scanivalve DSA3217 pessure sensors were used to obtain static pressure measurements from the sixteen pressure taps located on the surface of the airfoil(see 2.1). Overall, 100 data points were taken at a frequency of $20Hz$.

### 3.2 Hot Wire Anemometry

In order to obtain the power spectra that would reveal the most dominant frequencies in the flow, Hot Wire Anemometry(HWA) was used. The system consisted of a Dantec Dynamics MiniCTA 5442 bridge with a National Instruments IN USB-9162 data acquisition system. The resultant of the streamwise and vertical velocity components was measured using a single-sensor 55P15 boundary layer probe which allowed to obtain measurements very close to the surface of the airfoil. A traversing system, using the coordinate system shown in Figure 5, was used to position the probe at the desired point of measurement. The lines of measurement on the airfoil were placed perpendicular to the surface of the airfoil at $x/c = 0.1$, 0.2 and 0.3 denoted by $L1$, $L2$ and $L3$ respectively. Two measurement lines in the wake were also considered, placed perpendicularly to the freestream flow and denoted by $W1$ and $W2$. The position of $W1$ was $x/c = 0.033$ and $W2$ at $x/c = 0.1$, both measured from the trailing edge of the airfoil. The positions of the measurement lines are shown in Figure 5.

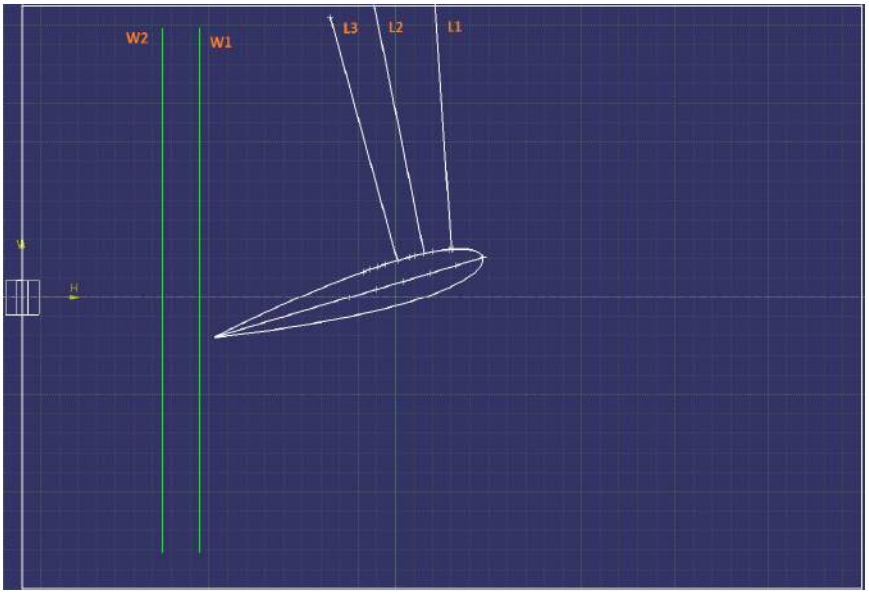


Figure 5: Location of measurement lines used to obtain power spectra of flow instabilities without actuation

The data were acquired at a frequency of $8kHz$ for a total test time of $5sec$ which results in 40000 data at each point along the measurement lines. The choice of frequency was such that the Nyquist criterion was satisfied.[26] For the measurement lines $L1$, $L2$ and $L3$, 40-70 points were examined at a $\Delta z = 0.5mm$. Likewise, for the measurement lines $W1$ and $W2$, 39-65 points were examined at a $\Delta z = 2.9mm$.

### 3.3 Particle Image Velocimetry

The PIV measurements were done using a LaVision PIV system. Illumination was handled by a Quantel Evergreen 200 double-pilse Nd:YAG laser which offers a $200mJ$ light pulse at a wavelength of $532nm$. The lens was adjusted such that the light sheet formed was parallel with the freestream flow and covered the entire chord of the airfoil, with a thickness of $1.2mm$. The images were acquired using a LaVision Imager SX 4M camera, equipped with a Nikon lens with a focal length of $28mm$. The time separation was set to $20\mu sec$ for both velocities tested. Finally, the flow was seeded using non-toxic DEHS(Di-2-Ethylhexyl-Sebacat) using an aerosol generator to produce particles with a mean diameter of $1.6\mu m$.

In order to get a more accurate picture of the flow field structures caused by the actuation, phase-locked PIV measurements were done. The timing was handled by a LaVision Programmable Timing Unit, which received its triggering signal by the same function generator used for the DBD actuator. Since the maximum trigger rate of the laser system was limited to $15Hz$, it was not possible to capture an image-pair at every actuation of the DBD. Therefore, an image-pair was acquired after a certain number of DBD actuations, depending on the frequency of actuation of the test case in question. Overall, 500 image-pairs were utilized to provide instantaneous velocity fields as well as time-averaged quantities. After the image acquisition, each image pair was processed using DaVis 8.2.0 with a decreasing

window size(64x64-32x32) multi-pass processing with a 50% overlap for the 64x64 window size and 75% overlap for 32x32.

## 4. Results

### 4.1 Spectral analysis without actuation

In order to identify the dominant frequencies present in the flow field, hot wire measurements were done along measurement lines (see Figure5). For consistency the points where the Power Spectral Density was calculated were the points where the peak RMS velocity was located, as seen in Figure 6.

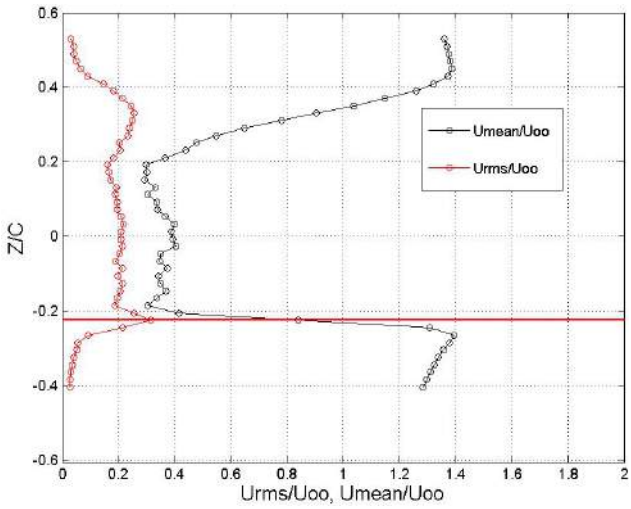


Figure 6: Example of the location where PSD analysis took place

It was found that along the measurement lines of $L1$, $L2$ and $L3$ the frequencies representing the shear layer and the wake vortex were present. The high shear layer characteristic frequencies are seen in the bulk of the PSD, whereas the low wake vortex characteristic frequencies are obvious as a peak. When comparing the shear layer frequencies along $L1$, $L2$ and $L3$ it was observed that there was a reduction in the frequency of the bulk which represents the characteristic frequency of the shear layer when moving downstream. The same wake vortex frequencies were also observed on $W1$ and $W2$. Based on the observed power spectra generated, the frequencies at which the actuation would be tested were finalised. An example of the power spectra can be seen in Figure 7 and Figure 8.

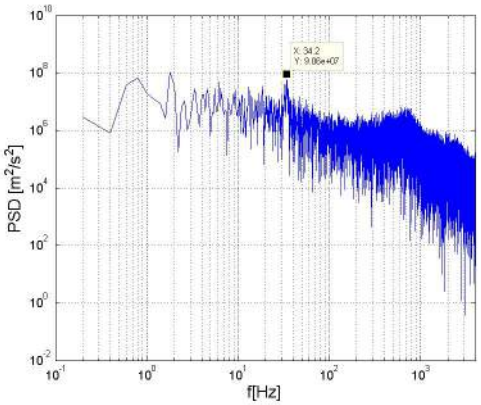


Figure 7: Power spectra along L1, $Re = 100000$ $\alpha = 24°$

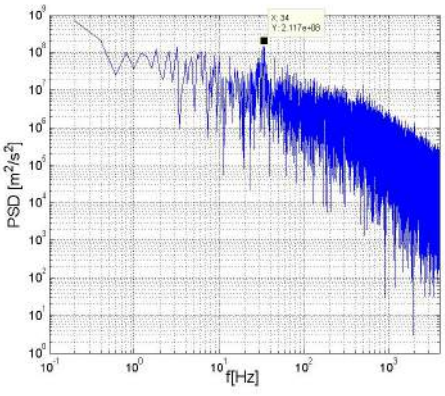


Figure 8: Power spectra along W2, $Re = 100000$ $\alpha = 24°$

According to the obtained power spectra, the most dominant and characteristic frequencies of the flow without plasma actuation were determined. The results of this analysis at a $Re = 100000$ and $\alpha = 16°$ determined that the most

dominant characteristic frequencies of the wake were $f = 35, 44.2\,Hz$, whereas for the shear layer the most dominant frequencies were 500 and 1058 $Hz$. At the same $Re$ and $\alpha = 24°$ the characteristic frequencies detected were $f = 34$, 203, 400 and 700 $Hz$.

At a $Re = 200000$ and $\alpha = 16°$ the frequencies detected in the power spectra were $f = 33.6$, 41, and 174.4 $Hz$. At the same $Re$ and $\alpha = 24°$ the frequencies found were $f = 69$, , 266.6, 470 and 1333.3 $Hz$. In all the cases the most dominant characteristic frequencies detected were used as the actuation frequency of the DBD actuator to determine the degree of control authority they posses in re-attaching separated flows at the respective angles of attack where they were detected.

### 4.2 Pressure Measurements with DBD actuation

In order to test the effectiveness of the dominant characteristic flow frequencies when used as an actuation frequency, the first criterion used was the pressure distribution along the airfoil. This would indicate which frequencies are most adept at re-attaching the separated flow.

#### 4.2.1 Early post-stall $\alpha = 16°$

This case was tested for $Re = 100000$ and $Re = 200000$ at all the dominant characteristic frequencies detected from the power spectra, as well as values of reduced frequency $F_c^+ = 1, 2, 3, 4$ and $F_c^+ = 10$ in the case of $Re = 100000$ and $F_c^+ = 1, 2$ and $F_c^+ = 4$ in the case of $Re = 200000$. The resulting pressure distributions can be seen below in Figure 9 and Figure 10.

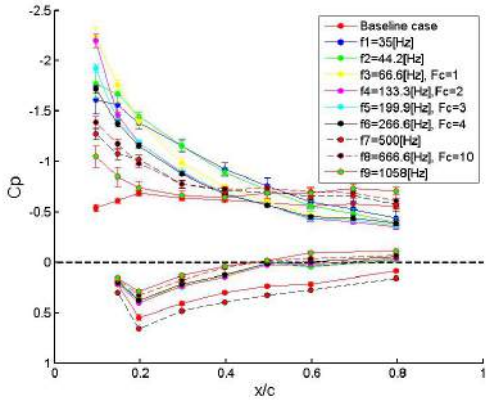


Figure 9: $C_p$ distribution at $U_\infty = 10m/s$, $\alpha = 16°$

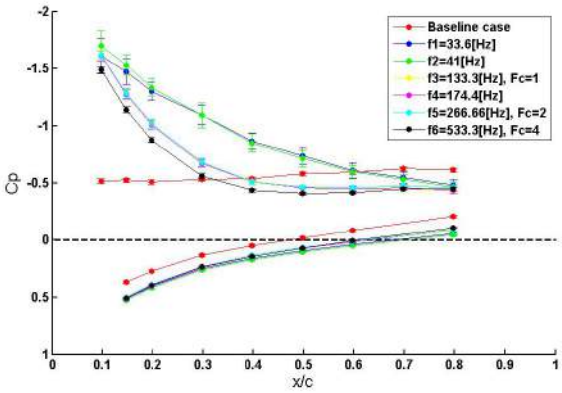


Figure 10: $C_p$ distribution at $U_\infty = 20m/s$, $\alpha = 16°$

In the case of $Re = 100000$, the actuation frequencies that produced the highest peak on the suction side of the airfoil were $F_c^+ = 1$ and 2, as is well established by literature. The actuation frequencies of $f = 35, 44.2\,Hz$, which were obtained from the power spectra, also showed promising control authority, whereas the higher actuation frequencies had poor performance. Furthermore, it is observed that when the DBD was actuated at $f = 35, 44.2\,Hz$ the area under the curve is increased, although no conclusions can be made since lift measurements were not obtained. Note, that the phenomenon of re-attachment is unstable as shown by the error bars on the graph.

Surprisingly, at $Re = 200000$ the highest suction peak was produced when the DBD was actuated at the characteristic frequencies of the wake and in particular $f = 41\,Hz$. As before, it is observed that the area under the curve is larger when the DBD is actuated at the dominant frequencies of the wake, compared to actuation frequencies of $F_c^+ = 1$ and 2. However, the fluctuations of the pressure readings are higher in the case of $f = 33.6$ and 41 $Hz$.

#### 4.2.2 Late post-stall $\alpha = 24°$

Again, this case was tested at same $Re$ as before. In the case of $Re = 100000$ besides the characteristic flow frequencies obtained from the power spectra, values of $F_c^+ = 1, 2, 3$ and 4 were tested. Similarly, in the case of $Re = 200000$ tested frequencies also included values of $F_c^+ = 1, 2, 3, 4$ and 10. The resulting $C_p$ distributions are shown in Figure 11 and Figure 12.

In both cases the DBD actuator showed no significant control authority in re-attaching the separated flow, except in the case of $Re = 200000$ and an actuation frequency of $f = 266.6\,Hz$ which corresponds to $F_c^+ = 2$. The only

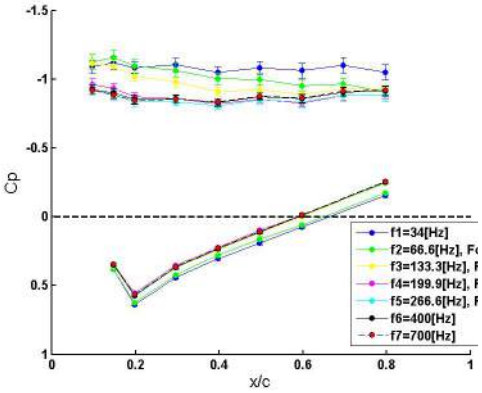


Figure 11: $C_p$ distribution at $U_\infty = 10m/s$, $\alpha = 24°$

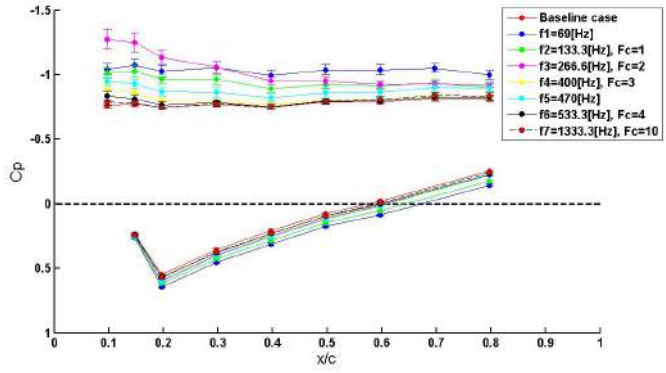


Figure 12: $C_p$ distribution at $U_\infty = 20m/s$, $\alpha = 24°$

phenomenon observed was the increase of the $C_p$ value on the suction side of the airfoil which is as more obvious when the DBD was actuated at the lowest values of the characteristic flow frequencies obtained from the power spectra.

### 4.3 Spectral analysis at specific DBD actuation frequencies

In order to determine the influence of the DBD actuation frequency on the existing characteristic structures of the flow, hot wire measurements were obtained at $W2$ using again as a criterion for the choice of point of measurement the location of the RMS velocity peak.

When the DBD is actuated at the same frequency as a dominant characteristic flow frequency without plasma actuation, it seems there is an increase in the magnitude of the PSD peak which can be seen in Figure 14. This increase of the magnitude was observed in all $Re$ and both angles of attack. Another interesting phenomenon which can be seen in Figure, is the presence of another PSD peak at much higher frequencies, on the order of 2000, $Hz$, which is observed only in certain actuation frequencies. The reason for the presence of this peak is unknown and will be the subject of further investigation.

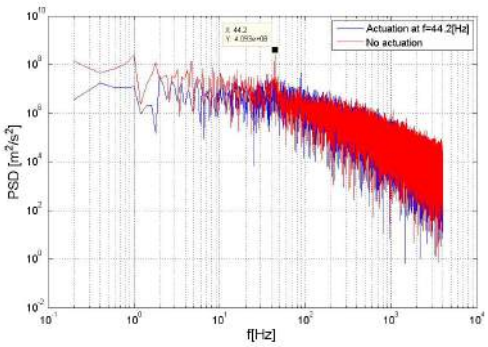


Figure 13: PSD analysis at $Re = 100000$ and $\alpha = 16°$

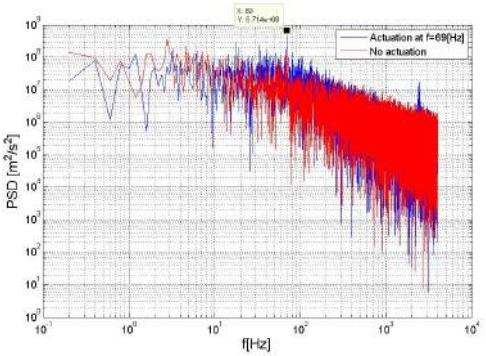


Figure 14: PSD analysis at $Re = 200000$ and $\alpha = 24°$

Another interesting phenomenon is observed when examining Figure 15, is the presence other frequency peaks when the DBD is actuated, which are multiples of the actuation frequency. The phenomenon of observing the multiples of the actuation frequency is observed in all other test cases as well. In order to disqualify this phenomenon as a measurement error, HWA measurements were performed in stagnant flow with DBD actuation where the power spectra retrieved showed no peaks at the frequency of actuation nor its multiples.

Since, other literature on the subject of plasma flow control mentions that the best actuation frequency for the DBD is $F_c^+ = 1$ to 2, an investigation was made using the power spectra. Studying the effects of actuating the DBD at the dominant characteristic frequencies involved comparing the power spectra when the DBD is actuated at $F_c^+ = 1$ and the best performing dominant characteristic frequency. The best data for this comparison where obtained at $Re = 200000$

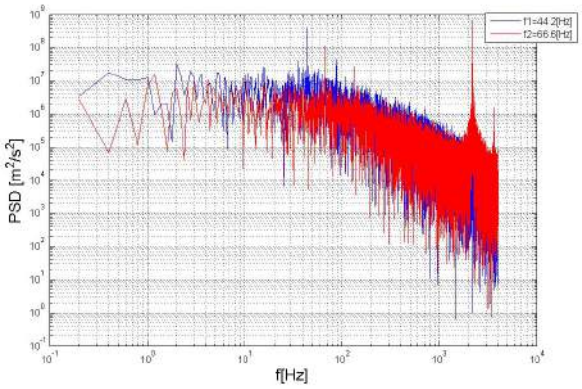


Figure 15: Power spectra showing multiples of actuation frequency at $Re = 100000$ and $\alpha = 16°$

and are shown in Figure 16 and Figure 17. At $\alpha = 16°$ where the pressure distribution shows the best performing actuation frequency is $f = 41\,Hz$ , the power spectra shows a higher PSD magnitude when compared to an actuation frequency of $133.3\,Hz$ which corresponds to $F_c^+ = 1$ . Again, notice that the multiples of the actuation frequency are present in the power spectra. Examining Figure 17, the same trend is present. At this angle of attack, the only frequency of actuation that has a significant effect on the pressure distribution is $f = 266.6\,Hz$ which corresponds to $F_c^+ = 2$. Comparing this actuation frequency equal characteristic flow frequency, it is observed that the lower actuation frequency is not obviously present in the power spectra. Compared to an actuation frequency of $f = 266.6\,Hz$ the difference in magnitude is quite large. Therefore, a correlation seems to exist between the magnitude of the PSD peak and the effectiveness of the DBD in re-attaching a separated flow over an airfoil.

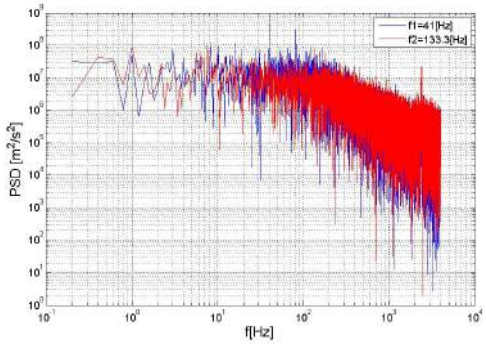


Figure 16: Power spectra at $Re = 200000$ and $\alpha = 16°$

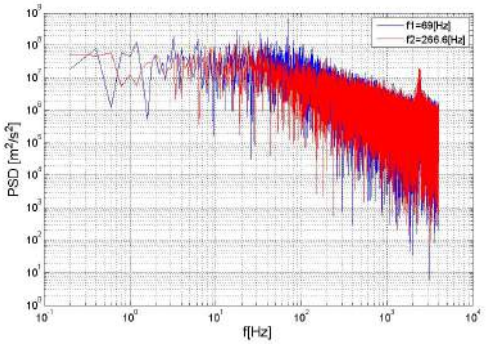


Figure 17: Power spectra at $Re = 200000$ and $\alpha = 24°$

### 4.4 Influence of applied voltage

Two values of voltage were used to produce plasma, specifically $4kV$ and $7kV$, in order to study the effects of applied voltage on the control authority of the DBD. The results gave contradictory data, which requires further investigation. Repeatability problems are not inferred.

As seen in Figure 18, at $\alpha = 16°$ and $Re = 100000$ increasing the applied voltage has a negative effect as the suction peak when $7kV$ are applied is quite lower compared to $4kV$. When analysing the power spectra of this test case, shown in Figure 19, it is observed that the peak at the actuation frequency of $66Hz$ is higher at $7kV$, however the multiple of the actuation frequency at $122Hz$ shows a higher peak for a $4kV$ applied voltage. However at the same angle of attack and $Re = 200000$ there seems to be little difference in pressure distributions although the PSD peak at the actuation seems to be more pronounced at an applied voltage of $7kV$, as seen in Figure 21 and Figure 20.

At $\alpha = 24°$ the findings seem to contradict the observation at $\alpha = 16°$. Here at a $Re = 100000$ applying $7kV$ of voltage results in a better pressure distribution, although the flow over the airfoil is still not attached, as seen in Figure22. When examining the pressure distribution at $Re = 200000$, shown in Figure 23, the better performing applied voltage is $4kV$.

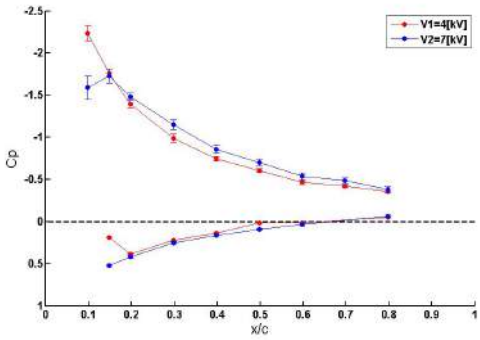


Figure 18: $C_p$ distribution comparing applied voltages at $Re = 100000$ and $\alpha = 16°$, actuation frequency $f = 66.6\,Hz$

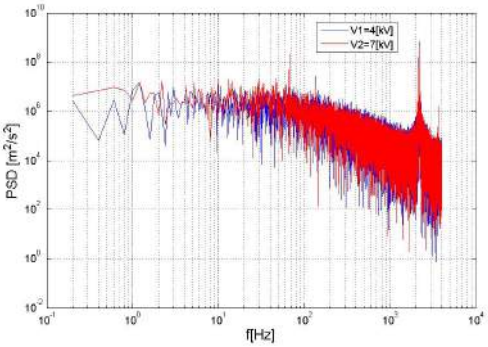


Figure 19: PSD analysis comparing applied voltages at $Re = 100000$ and $\alpha = 16°$, actuation frequency $f = 66.6\,Hz$

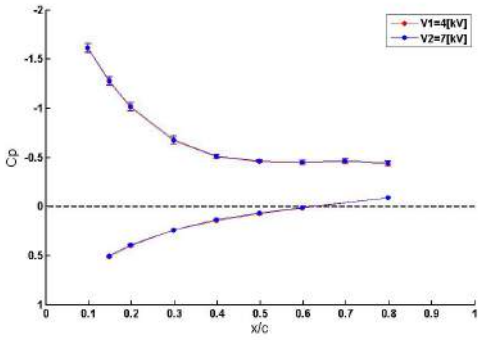


Figure 20: $C_p$ distribution comparing applied voltages at $Re = 200000$ and $\alpha = 16°$, actuation frequency $f = 174.4\,Hz$

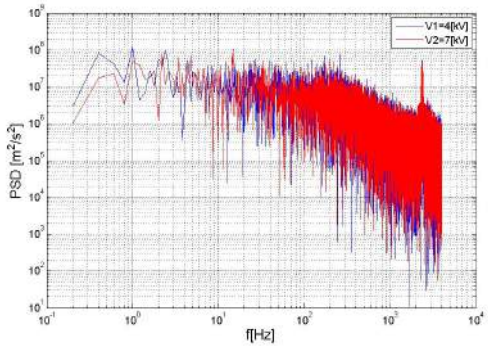


Figure 21: PSD analysis comparing applied voltages at $Re = 200000$ and $\alpha = 16°$, actuation frequency $f = 174.4\,Hz$

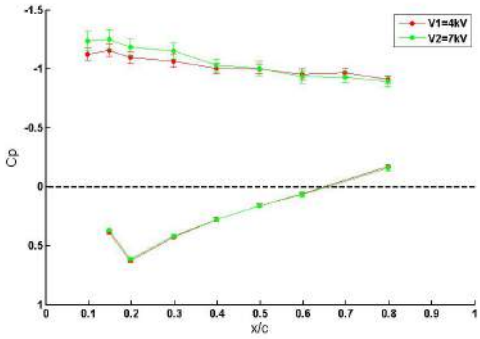


Figure 22: $C_p$ distribution comparing applied voltages at $Re = 100000$ and $\alpha = 16°$, actuation frequency $f = 66.6\,Hz$

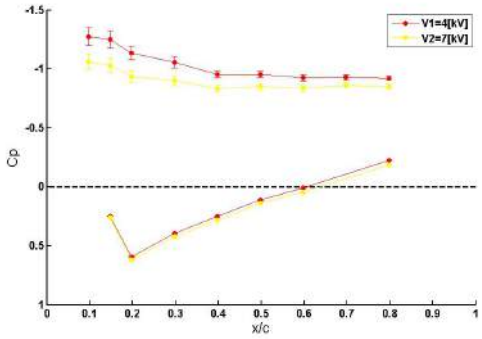


Figure 23: $C_p$ distribution comparing applied voltages at $Re = 200000$ and $\alpha = 16°$, actuation frequency $f = 266.6\,Hz$

### 4.5 PIV Measurements

Phase-locked PIV measurements can offer an inside at the specifics of the control mechanisms behind Ns-DBD actuators. The objective of this analysis was to observe the evolution of the flow over the airfoil when the DBD is active and to study the effect of different actuation frequencies on the structures of the flow.

It has been mentioned already that the phenomenon of re-attachment is an unstable phenomenon, which was shown by the pressure distributions obtained. In order to study how this instabilities evolve in time, the streamlines from six consecutive instantaneous velocity fields were produced. Each image pair obtained has a phase difference of 3600° with the actuation of the DBD, meaning that an image pair is obtained every ten actuations of the DBD. It is observed from Figure 24 that the flow over the airfoil is unstable, and therefore attaches and de-attaches at different time instances. Furthermore, the mechanism at work behind this instability seems to be the formation of a large vortex at the mid-chord of the airfoil. When the particular vortical structure breaks down the flow re-attaches again. Note that the Reynolds number for the flow evolution presented is 100000 and the actuation of the DBD is at $F_c^+ = 1$.

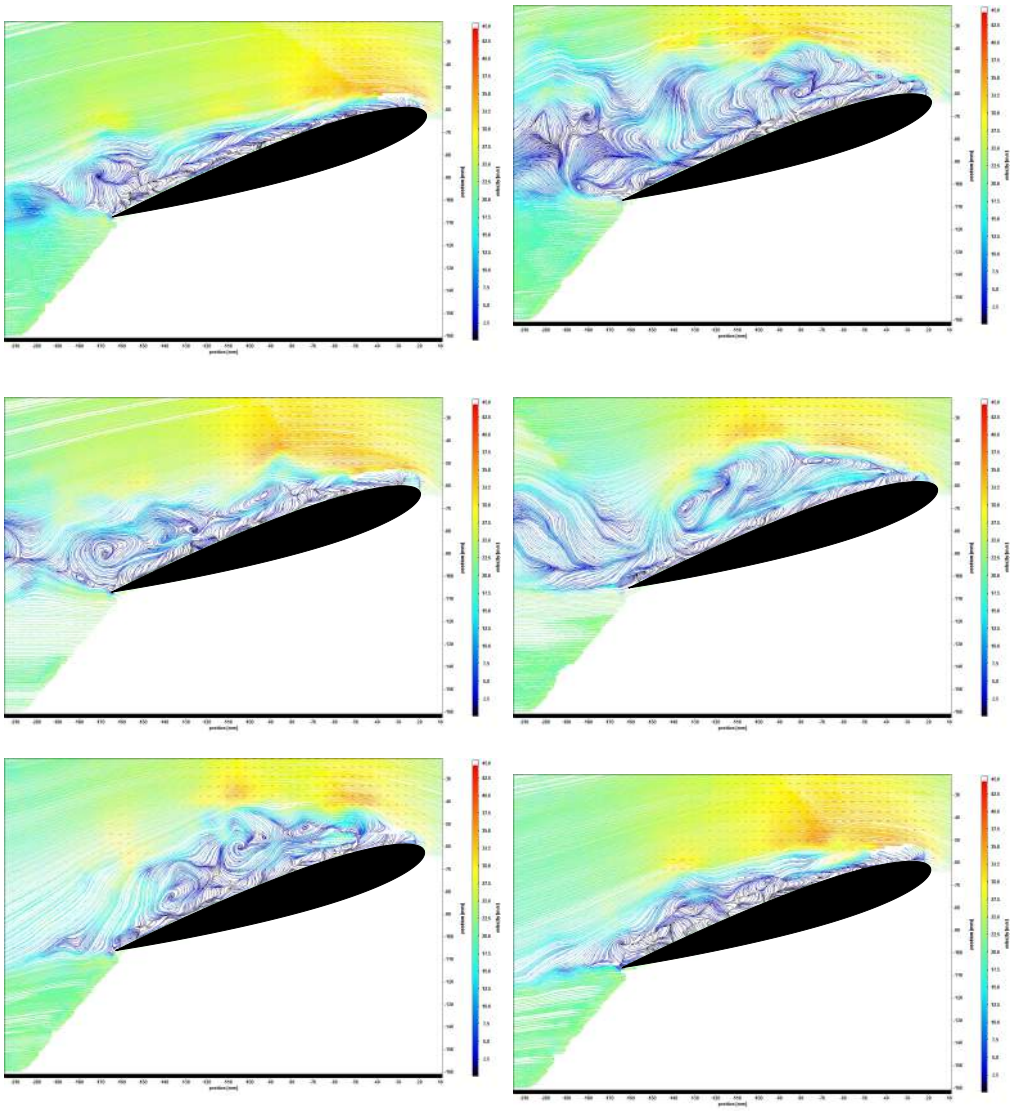

Figure 24: Evolution of flow instabilities with plasma actuation at $F_c^+ = 1$, $Re = 100000$.

However, the existence of this instability seems to be correlated with the Reynolds number. At the same actuation frequency of $F_c^+ = 1$ but at $Re = 200000$ this instability is not observed. Furthermore, this actuation frequency is observed to produce better results at a higher $Re$, since as seen in Figure 25 and Figure 26 the size of the wake is considerably decreased at the higher $Re$.

To get a better understanding as to how the DBD actuator influences the existing characteristic structures in the

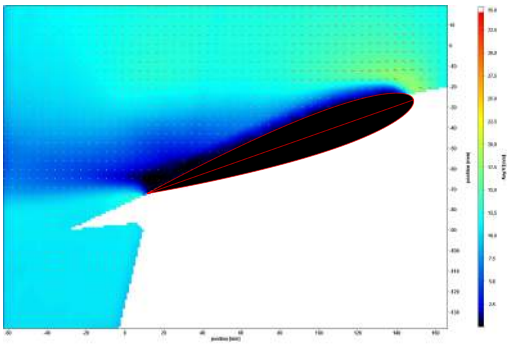

Figure 25: Velocity field at $Re = 100000$ and $\alpha = 16°$ and DBD actuation at $F_c^+ = 1$

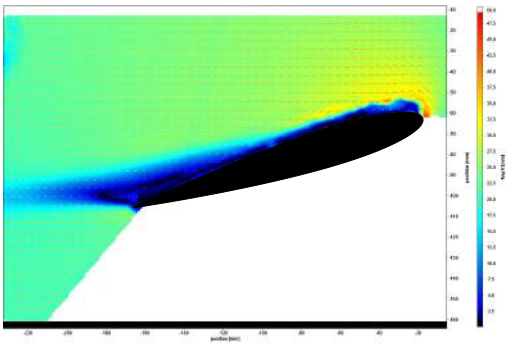

Figure 26: Velocity field at $Re = 200000$ and $\alpha = 16°$ and DBD actuation at $F_c^+ = 1$

flow field, images were taken at $\alpha = 24°$ and $Re = 200000$ where the instabilities were lower and the changes in the flow structure more pronounced. After the acquisition of 500 image-pairs, a time-averaged representation of the swirling strength was obtained. The frequencies of actuation used for the DBD were $69Hz$ and $266.6Hz$, of which the latter corresponds to $F_c^+ = 2$. Note that the frequency of $69Hz$ is a characteristic frequency of the flow which was obtained through analysis of the power spectra. As seen in Figure 27, at this frequency the structure that is most likely excited is the separation vortex. Compared to Figure 28, where the actuation frequency is $266.6Hz$ it is observed that different excitation mechanism exists which forms distinct vortical structures which diffuse as they move downstream in the direction of the flow.

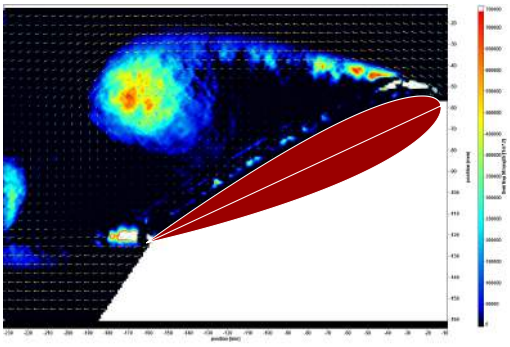

Figure 27: Swirling strength at actuation frequency of $69Hz$, $Re = 200000$ and $\alpha = 24°$

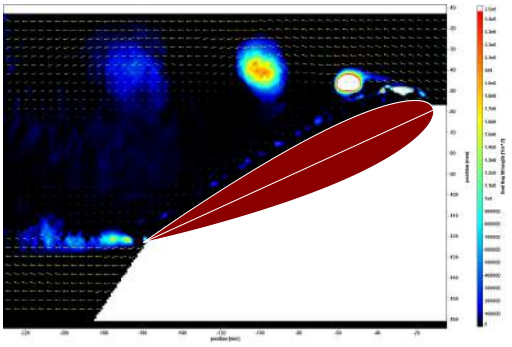

Figure 28: Swirling strength at actuation frequency of $266.6Hz$, $Re = 200000$ and $\alpha = 24°$

## 5. Conclusions

This paper the mechanisms that allow for control authority for an asymmetric nanosecond pulsed dielectric barrier discharge (NS-DBD) actuator on the aerodynamic characteristics of a NACA 0015 airfoil profile were investigated. Experiments were performed in a low-speed wind tunnel at freestream flow speeds of 10 and $20\,m/s$ at angles of attack of 16° and 24°. Pressure taps along the profile chord located at mid-span on both the suction and pressure sides of the airfoil were used also to determine the effectiveness of the actuator at various frequencies. Hot wire anemometry was performed with the aim of identifying dominant frequencies in the flow field over the stalled profile. Furthermore, PIV measurements were taken to identify how different actuation frequencies affect the existing structures in the flow field.

Through hot wire measurements without DBD actuation at different measurement lines along the airfoil and in the wake, the dominant characteristic flow frequencies were obtained. These frequencies were used as an actuation frequency for the DBD and were compared to known effective values of reduced frequency $F_c^+$. The degree of control authority that each actuation frequency was assessed by examining the pressure distributions along the airfoil. This analysis revealed that actuating the DBD at the low characteristic flow frequencies, the control authority at re-attaching the flow was significant, and in the case of $\alpha = 16°$ and $Re = 200000$ bettering the performance of actuation frequencies of $F_c^+ = 1$ and 2 which were known to be effective. Furthermore, at this angle of attack the area under the curve of the

pressure distribution was increased at the low characteristic frequencies. Actuating the DBD at the high characteristic flow frequencies produced some effect which was not significant.

When the most effective frequencies were identified based on pressure distributions, further power spectra were obtained with actuation. This revealed that when the DBD is actuated at a characteristic flow frequency, the magnitude of the PSD peak is increased. Furthermore, the multiples of the actuation frequency were observed in the power spectra. By comparing the power spectra of different actuation frequencies it was observed that the most effective frequency also produces a higher PSD peak.

By examining the PIV measurements, it was confirmed that the phenomena which occur with DBD actuation are unstable depending on the Reynolds number. Furthermore, it was observed that depending on the actuation frequency, different flow structures are excited and therefore the actuation frequency is critical to the control authority of a Ns-DBD actuator.

In conclusion, nanosecond-pulsed plasma actuators obtain their control authority via several mechanisms, not only limited to an equivalent energy transfer, nor on the micro-shockwave that emanates from the actuator[15,17] but particularly on the effect of relating characteristic flow frequencies to the actuation frequencies. This shows that further applications can be considered that were not yet suggested in the literature, giving a promising future for these actuators.

## References

[1] Prandtl, L. 1904. Über Flüssigkeitsbewegung bei sehr kleiner Reibung. *Proc. Third Int. Math. Congr. Heidelberg, Germany*, 484-491.

[2] Lachmann, G.V. 1961. Boundary Layer and Flow Control. Its Principles and Application, Volume 1. Pergamon Press.

[3] Gad-el-Hak, M. 1996. Modern developmenst in Flow Control. *Applied Mechanics Reviews*, vol. 49, pp. 365-379.

[4] Crowther, W. J. 2006. Separation Control on a Trailing-Edge Flap Using Air Jet Vortex Generators. *Journal of Aircraft*, 43(5):1589-1593.

[5] McLean, J.D., Crouch, J.D., Stoner, R.C., Sakurai, S., Seidel,G.E., Feifel, W. M. and Rush, H. M. 1999. Study of the Application of Separation Control by Unsteady Excitation to Civil Transport Aircraft. Technical Report NASA CR-1999-209228.

[6] Cattafesta, L. N. and Sheplak, M. 2011. Actuators for Active Flow Control. *Annu. Rev. Fluid Mech*. 43:247-272.

[7] Wilkinson, S.P. 1990. "Interactive Wall Turbulence Control," in Viscous Drag Reduction in Boundary Layers, eds. D.M. Bushnell and J.N. Hefner, *Progress in Astronautics and Aeronautics,, AIAA, Washington, D.C.*, vol. 123, pp. 479-509.

[8] Corke, T.C., Lon Enloe, C., and Wilkinson, S.P. 2010. Dielectric Barrier Discharge Plasma Actuators for Flow Control. *Annual Review of Fluid Mechanics* Vol. 42:505-529.

[9] Seifert, A., Darabi, A. and I. Wygnanski. 1996. Delay of airfoil stall by periodic excitation. *Journal of Aircraft*, 33:691-698.

[10] Erfani, R., Erfani, T. Hale, C., Kontis, K. and S.V. Utyzhnikov. 2011. Optimization of induced velocity for plasma actuator with multiple encapsulated electrodes using response surface methodology. *49th AIAA Aerospace Sciences Meeting including the New Horizons Forum and Aerospace Exposition*;AIAA Paper 2011-1206.

[11] Caruana, D., Tropea, C., Hollenstein, Ch., Boeuf, J-P. and ed.Choi, K. S., 2013. PLASMAERO European Project. *ERCOFTAC special edition on Plasma Aerodynamics*; vol. 94.

[12] Starikovskii, A.Yu., Nikipelov, A.A., Nudnova, M.M., and D.V. Roupassov. 2009. SDBD plasma actuator with nanosecond pulse-periodic discharge. *Plasma sources science and technology*, 18(3):034015.

[13] Moreau, E. 2007. Airflow control by non-thermal plasma actuators. *Journal of physics D: Applied physics*, 40:605-636.

[14] Patel, M.P., Ng, T.T., Vasudevan, S., Post, M.L., McLaughlin, T.E. and C.F. Suchomel. 2008. Scaling effects of an aerodynamic plasma actuator. *Journal of Aircraft*, 45:223-236.

[15] Roupassov, D. V., Nikipelov, A. A., Nudnova, M. M. and A. Yu. Starikovskii. 2009. Flow separation control by plasma actuator with nanosecond pulsed-periodic discharge. *AIAA Journal*, 47:168-185.

[16] Rethmel, C., Little, J., Takashima, K., Sinha, A., Adamovich, I. and M. Samimy. 2011. Separation control with nanosecond-pulse-driven dielectric barrier discharge plasma actuators. *49th AIAA Aerospace Sciences Meeting including the New Horizons Forum and Aerospace Exposition.* AIAA Paper 2011-487.

[17] Peschke, P., Goekce, S., Hollenstein, Ch., Leyland, P. and P. Ott. 2011. Interaction between nanosecond pulse DBD actuators and transonic flow. *42nd AIAA Plasmadynamics and Lasers Conference*. AIAA 2011-3734.

[18] Marino, A.; Peschke, P, De Gregorio, F., Leyland, P., Ott, P., Hollenstein, Ch., and Donelli, R. S. 2013. High Voltage Pulsed DBD Effects on the Aerodynamic Performances and on the Shock Buffet. *ERCOFTAC: Plasma Aerodynamics*, vol. 94, p. 70-76.

[19] Sidorenko, A.A., Zanin, B.Y., Postnikov, B.V., Budovksky, A.D., Starikovskii, A.Y., Roupassov, D.V., Zavialov, I.N., Malmuth, N.D., Smereczniak, P. and J.S. Silkey. 2007. Pulsed discharge actuators for rectangular wing separation control. *45th AIAA Aerospace Sciences Meeting and Exhibit*.AIAA Paper 2007-941.

[20] Little, J., Takashima, K., Nishihara, M., Adamovich, I. and M. Samimy. 2012. Separation control with nanosecond-pulse-driven dielectric barrier discharge plasma actuators. *AIAA Journal*, 50:350-365.

[21] Johnson, G.A. and S.J. Scott. 2001. Plasma-aerodynamic boundary layer interaction studies. *32nd AIAA Plasmadynamics and Lasers Conference and 4th Weakly Ionized Gases Workshop*.AIAA Paper 2001-3052.

[22] Grech, N. 2013. Investigation of flow separation control by nanosecond pulsed dielectric barrier discharge actuators at low flow speeds. Master Thesis. Ecole Polytechnique Fédérale de Lausanne.

[23] Peschke, P. 2014. Experimental Investigation of Pulsed DBD Plasma Actuators for Aerodynamic Flow Control. Ph. D Thesis, Ecole Polytechnique Fédérale de Lausanne.

[24] Lissaman, P.B.S. 1983. Low Reynolds number airfoils. *Annual Reviews of Fluid Mechanics*, 15:223-239.

[25] Kato, K., Breitsamter, C., Obi, S. (2014). Flow separation control over a GÃ¶ 387 airfoil by nanosecond pulse-periodic discharge. Experiments in Fluids, 55(8), 1-19.

[26] Bradshaw, Peter. An Introduction to Turbulence and Its Measurement: Thermodynamics and Fluid Mechanics Series. Elsevier, 2013.

[27] Geuns, R., Leyland, P., Plyushchev, G., Goekce, S., Peschke, P. 2014. Flow Separation Control with Plasma Actuators. Also in R. Geuns, Master Thesis TU Delft and Ecole Polytechnique Fédérale de Lausanne, Nov. 2014.